CSMA 2019
14ème Colloque National en Calcul des Structures
13-17 Mai 2019, Presqu'île de Giens (Var)

A FFT-based approach for Mesoscale Field Dislocation Mechanics: application to grain size effect in polycrystals

S. Berbenni[1], V. Taupin[2], R A. Lebensohn[2]

[1] *Université de Lorraine, CNRS, Arts et Métiers Paris Tech, LEM3, F-57000 Metz, France, {stephane.berbenni,vincent.taupin}@univ-lorraine.fr*
[2] *Theoretical Division, Los Alamos National Laboratory, Los Alamos, NM 87845, USA, lebenso@lanl.gov*

Résumé — A crystal elasto-viscoplastic FFT formulation coupled with the Mesoscale Field Dislocation Mechanics (MFDM) theory is presented. This MFDM-EVPFFT approach accounts for plastic flow and hardening from densities of geometrically necessary dislocations (GND) in addition to statistically stored dislocations (SSD). It is shown on 3D periodic Voronoi polycrystals that GND densities modify both intra-granular incompatible fields and stresses, which are at the origin of a grain size dependent flow stress of the Hall-Petch type.
Mots clés — crystal plasticity, elasto-viscoplastic, field dislocation mechanics, FFT, grain size effect.

1 Introduction

Numerical spectral approaches based on fast Fourier transform (FFT) algorithm have been recently proposed [1, 2, 3] for static Field Dislocation Mechanics (FDM) theory [4]. In the present contribution, an elasto-viscoplastic fast Fourier transform-based method (EVPFFT) for Mesoscale Field Dislocation Mechanics (MFDM) theory [5] is developed for describing grain size effects, slip constraints, flow stress due to both GND and SSD and local GND dislocation density evolutions in the course of monotonous plastic deformation of polycrystals (i.e. tensile deformation). Starting from the EVPFFT formulation [6], it is based on a novel expression of the Jacobian for the augmented Lagrangian scheme inferred from MFDM and on a numerical spectral resolution of the GND density evolution equation. Furthermore, the hardening model accounts for GND density and a geometric mean free path due to GND in addition to SSD classic hardening. Here, an interfacial jump condition on plastic distortion rate describing the conservation of Burgers vector for impenetrable grain boundaries is used [7, 8]. To numerically implement lattice incompatibility and integral Lippmann-Schwinger equations, discrete Fourier transform together with finite difference schemes are employed. Such numerical method has been revealed to be efficient for studying size effects in two-phase laminates [9].
The paper is organized as follows. In section 2, the constitutive equations of the Mesoscale Field Dislocation Mechanics (MFDM) are summarized and the elasto-viscoplastic FFT-based numerical implementation for MFDM, named MFDM-EVPFFT, is introduced. Section 3 is devoted to the numerical application of the MFDM-EVPFFT to faced-centered cubic (FCC) polycrystals with different grain sizes subjected to tensile loading. Grain size effects on the overall flow stress are reported as well as GND density and local stress profiles.

2 Field equations and numerical spectral method : MFDM-EVP-FFT approach

2.1 Field equations

To solve the displacement $\mathbf{u}$ and stress $\boldsymbol{\sigma}$ fields, the following equations are solved in a small deformation setting for elasto-viscoplastic materials with volume V with external boundary S using standard

traction/displacement boundary conditions on S_t and S_u ($S = S_t \cup S_u$) :

$$\begin{aligned} &\mathbf{div}\,\boldsymbol{\sigma} = 0 \\ &\boldsymbol{\sigma} = \mathbf{C} : (\mathbf{U}^e)^{sym} \\ &\mathbf{U} = \mathbf{grad}\,\mathbf{u} = \mathbf{U}^e + \mathbf{U}^p \\ &\boldsymbol{\sigma}\cdot\mathbf{n} = \mathbf{t}^0 \text{ on } S_t \\ &\mathbf{u} = \mathbf{u}^0 \text{ on } S_u \end{aligned} \tag{1}$$

where $\mathbf{C}$ is the fourth order elastic stiffness tensor with classic minor and major symmetries. In the presence of dislocation ensembles both the average plastic distortion $\mathbf{U}^p$, which results from dislocation motion, and the average elastic (or lattice) distortion $\mathbf{U}^e$ are incompatible fields. In non local crystal plasticity and depending on the resolution scale, dislocation ensembles can be categorized as GND (Geometrically Necessary Dislocations [11]) and SSD (Statistically Stored Dislocations). The mesoscale FDM theory (MFDM) is based on an average value of the dislocation density (or Nye) tensor $\boldsymbol{\alpha}$. Here, a simplified reduced version of the MFDM is considered [5, 10], where incompatible fields are assumed to be as smooth as necessary and the average plastic distortion rate writes :

$$\dot{\mathbf{U}}^p = \boldsymbol{\alpha}\times\mathbf{v} + \mathbf{L}^p \tag{2}$$

The mobility of SSD is represented by the mesoscale plastic distortion rate denoted $\mathbf{L}^p$ where the averaging procedure was defined in [5]. The space-time evolution of the average dislocation density tensor $\boldsymbol{\alpha}$ is prescribed as :

$$\dot{\boldsymbol{\alpha}} = -\mathbf{curl}\,\dot{\mathbf{U}}^p \tag{3}$$

Constitutive specifications on the dislocation velocity $\mathbf{v}$ and on the slip distortion rate $\mathbf{L}^p$ are now given from thermodynamic considerations, see [5] for details. Furthermore, plastic flow incompressibility is considered from the fact that $L^p_{ii} = 0$ and $e_{ikl}\alpha_{ik}v_l = 0$. The GND velocity $\mathbf{v}$ is prescribed as follows :

$$\mathbf{v} = \frac{\mathbf{g}}{|\mathbf{g}|}v \quad \text{with} \quad v \geq 0 \tag{4}$$

where $\mathbf{g}$ is the glide force parallel to $\mathbf{v}$ and v is the magnitude of $\mathbf{v}$. The constitutive equation adopted for v is based on the Orowan law for GND mobile dislocations yielding :

$$v = \frac{\eta^2\, b}{N}\left(\frac{\mu}{\tau_c}\right)^2 \sum_{s=1}^{N} |\dot{\gamma}^s| \tag{5}$$

where N is the total number of slip systems ($N = 12$ for FCC metals), $\dot{\gamma}^s$ is the slip rate on slip system s, η is a material constant close to $1/3$ [11], b is the magnitude of the Burgers vector, τ_c is the shear strength and μ is the isotropic elastic shear modulus of the material. Furthermore, $\mathbf{g}$ writes in component form :

$$g_r = e_{ikr}\alpha_{jk}S_{ij} - e_{ikr}\alpha_{ik}\frac{S_{mn}\alpha_{np}(\alpha_{mp}-\alpha_{pm})}{\alpha_{ij}(\alpha_{ij}-\alpha_{ji})}, \tag{6}$$

where $S_{ij} = \sigma_{ij} - \frac{1}{3}\sigma_{kk}\delta_{ij}$ denotes the deviatoric stress tensor.

Plastic distortion rate tensor $\mathbf{L}^p$ due to slip from SSD is defined as :

$$\mathbf{L}^p = \sum_{s=1}^{N} \dot{\gamma}^s \mathbf{b}^s \otimes \mathbf{n}^s = \sum_{s=1}^{N} \dot{\gamma}^s \mathbf{m}^s, \tag{7}$$

where $\mathbf{m}^s$ is the crystallographic orientation tensor such that $\mathbf{m}^s = \mathbf{b}^s \otimes \mathbf{n}^s$. For each slip system s, the unit vector $\mathbf{b}^s$ denotes the slip direction and $\mathbf{n}^s$ the slip plane unit normal. The constitutive equation for $\dot{\gamma}^s$ introduced in eqs. 5 and 7 is given by a classic power law :

$$\dot{\gamma}^s = \dot{\gamma}^0 \left(\frac{|\tau^s|}{\tau_c}\right)^{1/m} sgn(\tau^s) \tag{8}$$

where m is the strain rate sensitivity of the material, $\tau^s = \mathbf{m}^s : \boldsymbol{\sigma}$ is the resolved shear stress, $\dot{\gamma}^0$ is the reference slip rate and τ_c is considered identical for all slip systems. The cumulated slip rate on all slip systems is given by :

$$\dot{\Gamma} = |\boldsymbol{\alpha} \times \mathbf{v}| + \sum_{s=1}^{N} |\dot{\gamma}^s| \tag{9}$$

The evolution law for the shear strength τ_c follows the same hypotheses as the strain-hardening model developed by [8, 9] :

$$\dot{\tau}_c = \theta_0 \frac{\tau_s - \tau_c}{\tau_s - \tau_0} \dot{\Gamma} + k_0 \frac{\eta^2 \mu^2 \, b}{2\,(\tau_c - \tau_0)} \left(\sum_{s=1}^{N} |\boldsymbol{\alpha} \cdot \mathbf{n}^s| \, |\dot{\gamma}^s| + \sum_{s=1}^{N} |\boldsymbol{\alpha} \cdot \mathbf{n}^s| \, |\boldsymbol{\alpha} \times \mathbf{v}| \right) \tag{10}$$

where τ_0 is the yield strength due to lattice friction (which is low for FCC metals), τ_s is the saturation stress, θ_0 is the stage II hardening rate for FCC metals, k_0 is related to a geometric mean free path due to GND forest on slip system s.

For the space-time evolution of the dislocation density tensor (see eq. 3), an explicit forward Euler scheme was derived to numerically solve this equation starting from an implicit backward Euler scheme together with a Taylor expansion at first order of $\alpha_{ij}^{t+\triangle t}$ where $\triangle t$ is the time step [12]. In contrast with classic crystal plasticity (CP) theories, the evolution equations for MFDM leads to a jump condition on plastic distorsion rate across a material interface modeling impenetrable or penetrable interfaces to dislocations, see [7]. In the case of impenetrable grain boundaries to dislocations, which corresponds to the modeling of completely constrained plastic flow at the interface, this condition becomes $\dot{\mathbf{U}}^p \times \mathbf{n} = 0$ according to [8]. The unit normals have been computed using Cartesian moments following the procedure indicated in [13].

2.2 MFDM-EVPFFT formulation

Here, an elasto-viscoplastic crystal plasticity formulation is adopted in a small deformation setting. Using a backward Euler implicit time discretization and the generalized Hooke's law, the expression of the stress tensor $\boldsymbol{\sigma}$ at $t + \triangle t$ is given by :

$$\boldsymbol{\sigma}^{t+\triangle t} = \mathbf{C} : \boldsymbol{\varepsilon}^{e,t+\triangle t} = \mathbf{C} : \left(\boldsymbol{\varepsilon}^{t+\triangle t} - \boldsymbol{\varepsilon}^{p,t} - \dot{\boldsymbol{\varepsilon}}^{p,t+\triangle t}(\boldsymbol{\sigma}^{t+\triangle t}) \triangle t \right), \tag{11}$$

In what follows, the supra-indices $t + \triangle t$ are omitted for sake of simplicity, and only the fields corresponding to the previous time step t will be explicitly indicated. The unknown total strain field $\boldsymbol{\varepsilon}$ is solved through an integral Lippmann-Schwinger equation for the unknown strain field $\boldsymbol{\varepsilon}$:

$$\varepsilon_{ij}(\mathbf{x}) = \langle \varepsilon_{ij} \rangle - \int_V \Gamma^0_{ijkl}(\mathbf{x} - \mathbf{x}') \tau_{kl}(\mathbf{x}') dV' \tag{12}$$

where $\langle \boldsymbol{\varepsilon} \rangle$ represents the average value of $\boldsymbol{\varepsilon}$ in V, Γ^0_{ijkl} is the modified Green tensor associated with the homogeneous elastic moduli $\mathbf{C}^0$ and $\tau_{ij} = \sigma_{ij} - C^0_{ijkl}\varepsilon_{kl}$ is the stress polarization field. In the following, eq. 12 is solved using a computationally efficient scheme based on FFT and augmented Lagrangian introduced by [14].

In the Fourier space, let $\boldsymbol{\xi}$ be the Fourier vector of magnitude $\xi = \sqrt{\boldsymbol{\xi} \cdot \boldsymbol{\xi}}$ and components ξ_i in a general three-dimensional Cartesian coordinate system setting. The complex imaginary number is denoted i and defined as $\mathrm{i} = \sqrt{-1}$. Let $\widehat{\boldsymbol{\varepsilon}}(\boldsymbol{\xi})$ and $\widehat{\boldsymbol{\Gamma}}^0(\boldsymbol{\xi})$ be, respectively, the Fourier transform of $\boldsymbol{\varepsilon}(\boldsymbol{x})$ and $\boldsymbol{\Gamma}^0(\mathbf{x})$. The Fourier transform of the integral Lippmann-Schwinger equation (eq. 12) yields :

$$\begin{aligned} &\widehat{\boldsymbol{\varepsilon}}(\boldsymbol{\xi}) = -\widehat{\boldsymbol{\Gamma}}^0(\boldsymbol{\xi}) : \widehat{\boldsymbol{\tau}}(\boldsymbol{\xi}) \; \forall \boldsymbol{\xi} \neq \mathbf{0} \\ &\widehat{\boldsymbol{\varepsilon}}(\mathbf{0}) = \langle \boldsymbol{\varepsilon} \rangle \end{aligned} \tag{13}$$

where $\widehat{\Gamma}^0_{ijkl}$ was given in [15]. The calculation of the modified Green tensor in the Lippmann-Schwinger equation is performed using a centered finite difference scheme on a rotated grid introduced by [16].

Let us assume now that $\lambda_{ij}^{(\mathrm{n})}$ and $e_{ij}^{(\mathrm{n})}$ are, respectively, the auxiliary guess stress and strain fields at iteration (n). The stress polarization tensor becomes : $\tau_{ij}^{(\mathrm{n})} = \lambda_{ij}^{(\mathrm{n})} - C^0_{ijkl} e_{kl}^{(\mathrm{n})}$. An alternative fixed-point

expression, which requires computing the Fourier transform of the stress field instead of that of the polarization field was reported in [14] :

$$\begin{aligned} \widehat{e}_{ij}^{(\mathrm{n}+1)}(\boldsymbol{\xi}) &= \widehat{e}_{ij}^{(\mathrm{n})}(\boldsymbol{\xi}) - \widehat{\Gamma}^0_{ijkl}(\boldsymbol{\xi})\widehat{\lambda}_{kl}^{(\mathrm{n})}(\boldsymbol{\xi}) \;\forall \boldsymbol{\xi} \neq \mathbf{0} \\ \widehat{e}_{ij}^{(\mathrm{n}+1)}(\mathbf{0}) &= \langle \varepsilon_{ij}^{(\mathrm{n})} \rangle \end{aligned} \tag{14}$$

Once $e_{ij}^{(\mathrm{n}+1)} = \mathrm{FFT}^{-1}(\widehat{e}_{ij}^{(\mathrm{n}+1)}(\boldsymbol{\xi}))$ is obtained in the real space by using the inverse Fourier transform (FFT^{-1}), the nullification of the residual $\mathbf{R}$, which depends on the stress and strain tensors $\boldsymbol{\sigma}^{(\mathrm{n}+1)}$ and $\boldsymbol{\varepsilon}^{(\mathrm{n}+1)}$, is solved :

$$R_{ij}(\boldsymbol{\sigma}^{(\mathrm{n}+1)}) = \sigma_{ij}^{(\mathrm{n}+1)} + C^0_{ijmn}\varepsilon_{mn}^{(\mathrm{n}+1)}(\boldsymbol{\sigma}^{(\mathrm{n}+1)}) - \lambda_{ij}^{(\mathrm{n})} - C^0_{ijmn}e_{mn}^{(\mathrm{n}+1)} = 0 \tag{15}$$

This nonlinear equation was solved by [6] using a Newton-Raphson-type scheme. The $(\mathrm{p}+1)$-guess for the stress field $\boldsymbol{\sigma}_{ij}^{(\mathrm{n}+1)}$ is given by :

$$\sigma_{ij}^{(\mathrm{n}+1,\mathrm{p}+1)} = \sigma_{ij}^{(\mathrm{n}+1,\mathrm{p})} - \left(\left(\frac{\partial R_{ij}}{\partial \sigma_{mn}} \right)_{\boldsymbol{\sigma}^{(\mathrm{n}+1,\mathrm{p})}} \right)^{-1} R_{mn}\left(\boldsymbol{\sigma}^{(\mathrm{n}+1,\mathrm{p})}\right) \tag{16}$$

Using the constitutive specifications, the Jacobian in the above expression reads :

$$\left(\frac{\partial R_{ij}}{\partial \sigma_{mn}} \right)_{\boldsymbol{\sigma}^{(\mathrm{n}+1,\mathrm{p})}} = \delta_{im}\delta_{jn} + C^0_{ijkl}C^{-1}_{klmn} + \triangle t\, C^0_{ijkl}\left(\frac{\partial \dot{\varepsilon}^p_{kl}}{\partial \sigma_{mn}} \right)_{\boldsymbol{\sigma}^{(\mathrm{n}+1,\mathrm{p})}} \tag{17}$$

The expression of $\partial \dot{\varepsilon}^p_{kl}/\partial \sigma_{mn}$ considering the constitutive equations of the MFDM theory yields [9] :

$$\left(\frac{\partial \dot{\varepsilon}^p_{kl}}{\partial \sigma_{mn}} \right)_{\boldsymbol{\sigma}^{(\mathrm{n}+1,\mathrm{p})}} = \frac{1}{2}\left(\frac{\partial L^p_{kl}}{\partial \sigma_{mn}} + \frac{\partial L^p_{lk}}{\partial \sigma_{mn}} \right)_{\boldsymbol{\sigma}^{(\mathrm{n}+1,\mathrm{p})}} + \frac{1}{2}\left(\frac{\partial (\alpha \times v)_{kl}}{\partial \sigma_{mn}} + \frac{\partial (\alpha \times v)_{lk}}{\partial \sigma_{mn}} \right)_{\boldsymbol{\sigma}^{(\mathrm{n}+1,\mathrm{p})}} \tag{18}$$

An approximation expression of $\partial L^p_{kl}/\partial \sigma_{mn}$ is given by :

$$\left(\frac{\partial L^p_{kl}}{\partial \sigma_{mn}} \right)_{\boldsymbol{\sigma}^{(\mathrm{n}+1,\mathrm{p})}} \simeq n\dot{\gamma}^0 \sum_{s=1}^{N} m^s_{kl}P^s_{mn}\frac{|P^s_{mn}\sigma_{mn}|^{n-1}}{(\tau_c)^n} \tag{19}$$

where $\mathbf{P}^s = (\mathbf{m}^s)^{sym}$. The determination of the expression of $\partial (\alpha \times v)_{kl}/\partial \sigma_{mn}$ is new compared to the standard EVPFFT formulation and is computed as follows [9] :

$$\left(\frac{\partial (\alpha \times v)_{kl}}{\partial \sigma_{mn}} \right)_{\boldsymbol{\sigma}^{(\mathrm{n}+1,\mathrm{p})}} = e_{lqr}\alpha_{kq}\left(\frac{\partial (g_r/|\mathbf{g}|)}{\partial \sigma_{mn}} v + \frac{g_r}{|\mathbf{g}|}\frac{\partial v}{\partial \sigma_{mn}} \right)_{\boldsymbol{\sigma}^{(\mathrm{n}+1,\mathrm{p})}} \tag{20}$$

with :

$$\begin{aligned} \frac{\partial (g_r/|\mathbf{g}|)}{\partial \sigma_{mn}} = &\left(\frac{\delta_{rs}|\mathbf{g}|^2 - g_r g_s}{|\mathbf{g}|^3} \right)\left(e_{oks}\alpha_{qk} - e_{iks}\alpha_{ik}\frac{\alpha_{qp}(\alpha_{op} - \alpha_{po})}{\alpha_{ij}(\alpha_{ij} - \alpha_{ji})} \right) \\ &\left(\delta_{om}\delta_{qn} - \frac{1}{3}\delta_{mn}\delta_{oq} \right) \end{aligned} \tag{21}$$

and :

$$\left(\frac{\partial v}{\partial \sigma_{mn}} \right)_{\boldsymbol{\sigma}^{(\mathrm{n}+1,\mathrm{p})}} \simeq n\dot{\gamma}^0 \frac{\eta^2\, b}{N}\left(\frac{\mu}{\tau_c} \right)^2 \sum_{s=1}^{N} P^s_{mn}\frac{|P^s_{mn}\sigma_{mn}|^{n-1}}{(\tau_c)^n} \tag{22}$$

In eqs. 19 and 22, the approximation lies in the fact that the derivatives $\partial \tau_c/\partial \boldsymbol{\sigma}$ and $\partial \mathbf{P}^s/\partial \boldsymbol{\sigma}$ are neglected.

Once the convergence is achieved on $\boldsymbol{\sigma}^{(\mathrm{n}+1)}$ and $\boldsymbol{\varepsilon}^{(\mathrm{n}+1)}$, the new guess for the auxiliary stress field $\boldsymbol{\lambda}$ is given by using the Uzawa descent algorithm :

$$\lambda_{ij}^{(\mathrm{n}+1)} = \lambda_{ij}^{(\mathrm{n})} + C^0_{ijkl}\left(e_{kl}{}^{(\mathrm{n}+1)} - \varepsilon_{kl}{}^{(\mathrm{n}+1)} \right) \tag{23}$$

and the algorithm is stopped when the normalized average differences between the stress fields $\boldsymbol{\sigma}$ and $\boldsymbol{\lambda}$, and the strain fields $\boldsymbol{\varepsilon}$ and $\mathbf{e}$, are smaller than a given threshold error (typically 10^{-5}). This condition implies the fulfillment of both stress equilibrium and strain compatibility up to sufficient accuracy.

In the algorithm described above, an overall macroscopic strain $\mathbf{E} = \langle \varepsilon^{(\mathrm{n})} \rangle$ is applied to the periodic unit cell V in the form of :

$$E_{ij} = E_{ij}^{t} + \dot{E}_{ij} \triangle t \tag{24}$$

In cases of mixed boundary conditions with imposed macroscopic strain rate $\dot{E}_{ij}$ and stress Σ_{ij}, the $(\mathrm{n}+1)$-guess of the macroscopic strain $E_{ij}^{(\mathrm{n}+1)}$ was given in [14, 6].

Let $\widehat{\boldsymbol{\alpha}}(\boldsymbol{\xi})$ be the Fourier transform of $\boldsymbol{\alpha}(\boldsymbol{x})$. Following [12, 9] :

$$\widehat{\alpha}_{ij}^{t+\triangle t} = \kappa(\eta) \left(\widehat{\alpha}_{ij}^{t} - \triangle t \, \mathrm{i} \, \xi_k \left(\widehat{(\alpha_{ij} v_k)}^{t} - \widehat{(\alpha_{ik} v_j)}^{t} \right) \right) - \triangle t \, \mathrm{i} \, \xi_k \, e_{jkl} \widehat{\left(L_{il}^{p}\right)}^{t} \tag{25}$$

where an exponential second order spectral low-pass filter was used to stabilize the numerical approximation of by eliminating high frequencies leading to spurious oscillations. The exponential filter is defined as function of discrete frequencies η as :

$$\kappa(\eta) = \exp\left(-\beta(\eta)^{2p}\right), \tag{26}$$

where the damping parameter β is defined as $\beta = -\log \varepsilon_M$, where ε_M is low value parameter that was optimized by [12]. For applications, $\varepsilon_M = 0.2$ and $p = 1$. To fix the time step $\triangle t$ in eq. 25 to satisfy stability requirements for numerically solving the dislocation density transport equation, a user-specified fraction denoted $c = 0.25$ of Courant-Friedrichs-Levy (CFL) limit is used in the numerical applications such that :

$$\triangle t_{CFL} = c \frac{\delta}{v_{max}} \tag{27}$$

where δ is the voxel size and v_{max} is the maximal GND velocity.

3 Application : grain size dependent behavior of FCC polycrystals

3.1 Material and simulation data

In the following numerical simulations, an elasto-viscoplastic Al polycrystal constituted of 27 grains resulting from periodic Voronoi tessellations is considered, see Fig. 1 (left). The crystallographic orientations of the grains are randomly distributed. As in [17], the average grain size d is deduced from $H/\sqrt[3]{27}$ where H is the period of the unit cell. The material parameters related to elastic constants (Al), slip rule, GND velocity ($\dot{\gamma}^0$, m and η) and hardening (τ_0, τ_s, θ_0 and k_0) were consistent with pure Al. Here, a specific fit to experimental data has not been carried out. The Burgers vector magnitude for Al is $b = 2.86 \times 10^{-10} m$. The reference material parameters used for numerical simulations are reported in Table 1. The unit cell is submitted to a tensile loading with mixed strain/stress boundary conditions and applied tensile strain rate is $\dot{E}_{33} = 0.001 s^{-1}$.

TABLE 1 – List of reference material parameters used for simulations

E (GPa)	ν	$\dot{\gamma}^0 (s^{-1})$	m	η	b (m)	τ_0 (MPa)	τ_s (MPa)	θ_0 (MPa)	k_0
69	0.33	1	0.05	0.33	2.86×10^{-10}	3	12	150	20

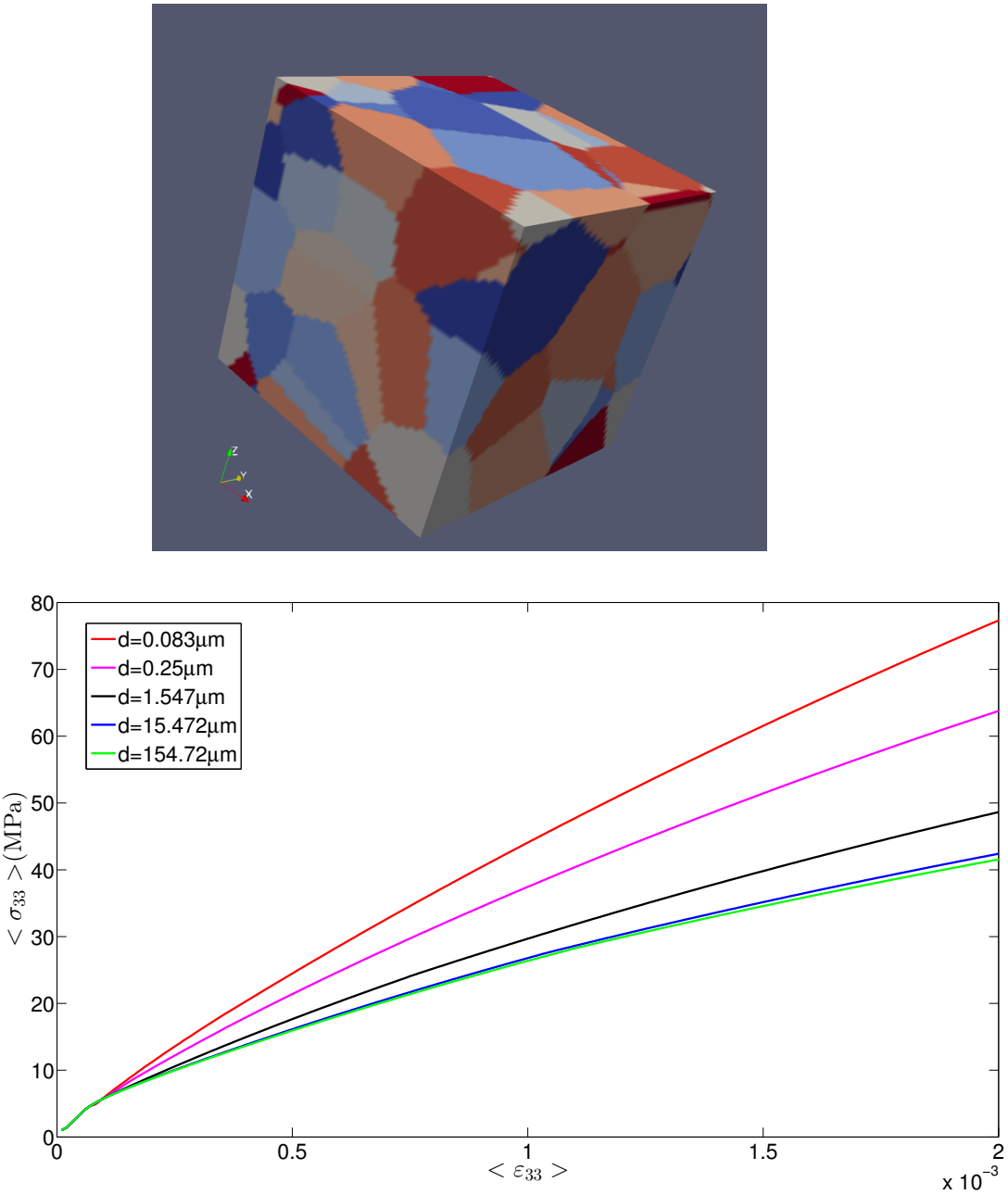

FIGURE 1 – (Top) : Periodic unit cell representing a Al polycrystal constituted of 27 grains resulting from Voronoi tessellations (64^3 voxels). A random crystallographic texture is used and the average grain size d varies from $0.083\mu m$ to $125.54\mu m$. A pure tensile deformation is applied to the unit cell with applied strain rate : $\dot{E}_{33} = 0.001s^{-1}$. (Bottom) : Grain size dependent tensile stress/strain curves obtained from present MFDM-EVPFFT approach for the different grain sizes d.

3.2 Results and discussion

The overall tensile stress ($< \sigma_{33} >$)/ tensile strain ($< \varepsilon_{33} >$) responses are reported on Fig. 1 (right). It is shown that the macroscopic tensile flow stress is grain size dependent and the scaling law for the flow stress at 0.2% strain is of Hall-Petch type : $< \sigma_{33} > \propto d^{-1/2}$. This grain size dependent behavior is due to the effect of GND density as reported in Fig. 2 (top) and associated non local plasticity inferred from MFDM-EVPFFT, which is at the origin of larger stress gradients compared to classic CP-EVPFFT (conventional size-independent plasticity), see Fig. 2 (bottom).

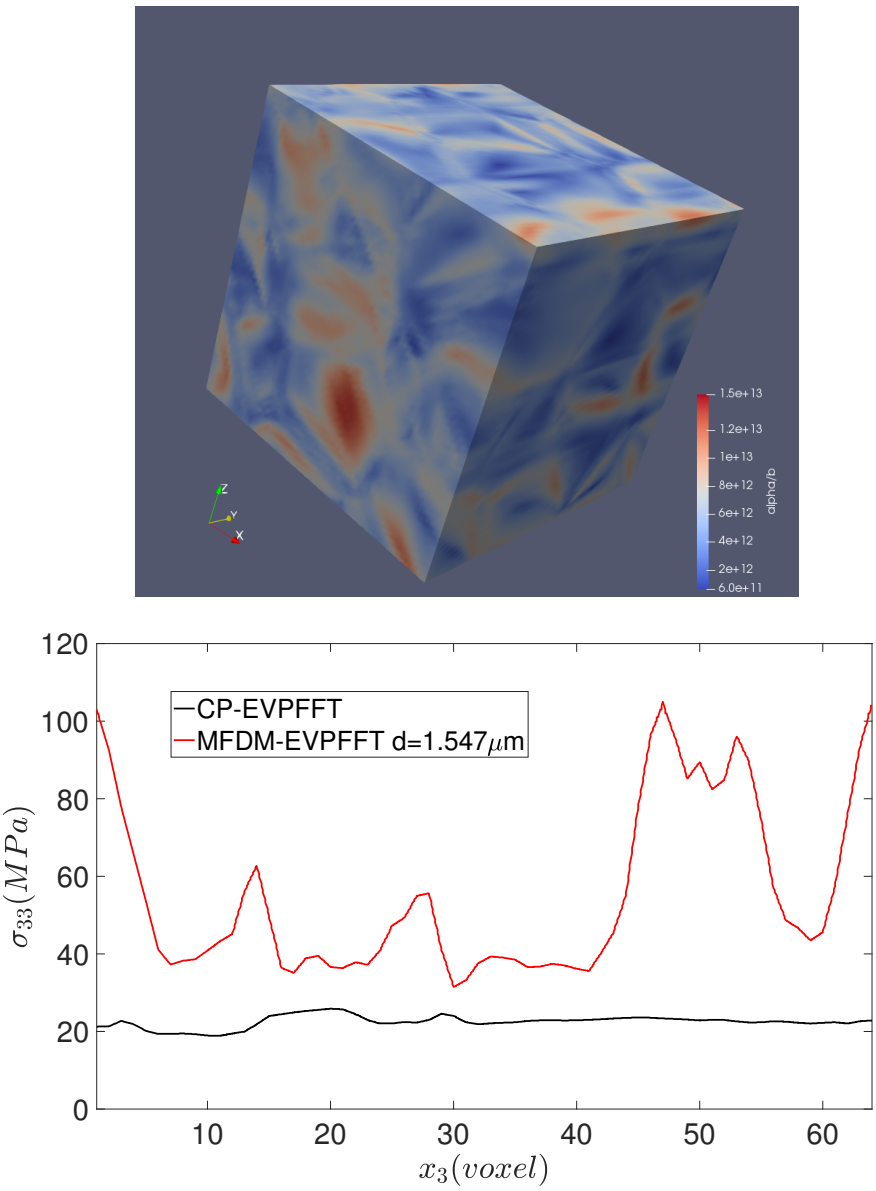

FIGURE 2 – (Top) : GND density $\rho_{GND} = \sqrt{\alpha_{ij}\alpha_{ij}}/b$ (m^{-2}) distribution in the unit cell at 0.2% strain for a polycrystal with grain size $d = 1.547\mu m$; (Bottom) : Spatial profile of stress component σ_{33} (MPa) in the x_3 direction crossing the center of the unit cell : comparison between classic CP-EVPFFT (grain size-independent) and MDFM-EVPFFT (grain size-dependent) (here $d = 1.547\mu m$).

Acknowledgements

SB, VT thank the French State (ANR) through the program “Investment in the future" (LabEx “DAMAS" referenced as ANR-11-LABX-0008-01) for financial support. RAL work was funded by Los Alamos National Laboratory LDRD program and US Department of Energy, Office of Basic Energy Sciences, project FWP 06SCPE401.

Références

[1] R. Brenner, A.J. Beaudoin, P. Suquet, A. Acharya. *Numerical implementation of static Field Dislocation Mechanics theory for periodic media*, Philos. Mag. 49, 1-24, 2014.

[2] S. Berbenni, V. Taupin, K.S. Djaka, C. Fressengeas. *A numerical spectral approach for solving elasto-static field dislocation and g-disclination mechanics*, Int. J. Solids Struct. 51, 4157-4175, 2014.

[3] K.S. Djaka, A. Villani, V. Taupin, L. Capolungo, S. Berbenni. *Field Dislocation Mechanics for heterogeneous elastic materials : A numerical spectral approach*, Comp. Meth. Appl. Mech. Eng. 315, 921-942, 2017.

[4] A. Acharya. *A model of crystal plasticity based on the theory of continuously distributed dislocations*, J. Mech. Phys. Solids 49, 761-784, 2001.

[5] A. Acharya, A. Roy. *Size effects and idealized dislocation microstructure at small scales : Predictions of a Phenomenological model of Mesoscopic Field Dislocation Mechanics : Part I*, J. Mech. Phys. Solids 54, 1687-1710, 2006.

[6] R.A. Lebensohn, A.K. .Kanjarla, P. Eisenlohr. *An elasto-viscoplastic formulation based on Fast Fourier Transforms for the prediction of micromechanical fields in polycrystalline materials*, Int. J. Plast. 32-33, 59-69, 2012.

[7] A. Acharya. *Jump condition for GND evolution as a constraint on slip transmission at grain boundaries*, Philos. Mag. 87, 1349-1359, 2007.

[8] S. Puri, A. Das, A. Acharya. *Mechanical response of multicrystalline thin films in mesoscale field dislocation mechanics*, J. Mech. Phys. Solids. 59, 2400-2417, 2011.

[9] K.S. Djaka, S. Berbenni, V. Taupin, R.A. Lebensohn. *A FFT-based numerical implementation of mesoscale field dislocation mechanics : application to two-phase laminates*, Int. J. Solids Struct. In Press, https ://doi.org/10.1016/j.ijsolstr.2018.12.027, 2019.

[10] A. Roy, S. Puri, A. Acharya. *Phenomenological mesoscopic field dislocation mechanics, lower-order gradient plasticity, and transport of mean excess dislocation density*, Modell. Simul. Mater. Sci. Eng. 15, 167-180, 2007.

[11] M.F. Ashby. *Deformation of plastically non-homogeneous materials*, Philos. Mag. 21, 399-424, 1970.

[12] K.S. Djaka, V. Taupin, S. Berbenni, C. Fressengeas. *A numerical spectral approach to solve the dislocation density transport equation*, Modell. Simul. Mater. Sci. Eng. 23, 065008, 2015.

[13] E.J. Lieberman, A.D. Rollett, R.A. Lebensohn, E.M. Kober. *Calculation of grain boundary normals directly from 3D microstructure images*, Modell. Simul. Mater. Sci. Eng. 23, 035005, 2015.

[14] J.C. Michel, H. Moulinec, P. Suquet. *A computational scheme for linear and non-linear composites with arbitrary phase contrast*, Int. J. Num. Meth. Eng. 52, 139-160, 2001.

[15] H. Moulinec, P. Suquet. *A numerical method for computing the overall response of nonlinear composites with complex microstructure*, Comput. Meth. Appl. Mech. Eng. 157, 69-94, 1998.

[16] F. Willot. *Fourier-based schemes for computing the mechanical response of composites with accurate local fields*, C. R. Meca. 343, 232-245, 2015.

[17] R.A. Lebensohn, A. Needleman. *Numerical implementation of non-local polycrystal plasticity using fast Fourier transforms*, J. Mech. Phys. Solids 97, 333-351, 2016.